

Article

An Improved Super-Twisting High-Order Sliding Mode Observer for Sensorless Control of Permanent Magnet Synchronous Motor

Yujiao Zhao ¹, Haisheng Yu ^{1,*} and Shixian Wang ²

¹ Shandong Province Key Laboratory of Industrial Control Technology, College of Automation, Qingdao University, Qingdao 266071, China; zhaoyujiao1225@163.com

² School of Mechanical, Electrical and Information Engineering, Shandong University at Weihai, Weihai 264209, China; 202017455@mail.sdu.edu.cn

* Correspondence: yhsh_qd@qdu.edu.cn; Tel.: +86-0532-85-953-972

Abstract: This article presents an improved super-twisting high-order sliding mode observer for permanent magnet synchronous motors to achieve high-performance sensorless control. The proposed observer is able to simultaneously estimate rotor position and speed, as well as track parameter disturbances online. Then, according to the back-EMF model, the sensorless observer is further constructed to improve the estimation effect. The estimated rotor position and speed are used to replace the actual values detected by the sensor, and the estimated parameter disturbances are considered as feedback values to compensate the command voltage. In this way, not only is the estimation accuracy improved, but the robustness against uncertainties is also enhanced. Simulation and experimental results show that the proposed observer can effectively track the rotor position and speed and obtain good dynamic and steady-state performance.



Citation: Zhao, Y.; Yu, H.; Wang, S. An Improved Super-Twisting High-Order Sliding Mode Observer for Sensorless Control of Permanent Magnet Synchronous Motor. *Energies* **2021**, *14*, 6047. <https://doi.org/10.3390/en14196047>

Academic Editor: Frede Blaabjerg

Received: 29 August 2021

Accepted: 17 September 2021

Published: 23 September 2021

Publisher's Note: MDPI stays neutral with regard to jurisdictional claims in published maps and institutional affiliations.



Copyright: © 2021 by the authors. Licensee MDPI, Basel, Switzerland. This article is an open access article distributed under the terms and conditions of the Creative Commons Attribution (CC BY) license (<https://creativecommons.org/licenses/by/4.0/>).

Keywords: super-twisting sliding mode observer; sensorless control; permanent magnet synchronous motor

1. Introduction

The permanent magnet synchronous motor (PMSM) incorporates the advantages of high efficiency, high power density, and simple structure, which is widely used in many highly dynamic and high-precision engineering applications, such as industrial drive, aerospace, electric vehicle, and so forth [1]. On the other hand, PMSM is a nonlinear control object affected by parameter uncertainties and external disturbances, which makes it difficult to obtain satisfactory performance during the entire operation [2–4]. The control performance can be improved by optimizing the machine design or applying advanced control strategies. Most control methods and modern control techniques require accurate position and speed information for field orientation and closed-loop control. It can be detected by mechanical sensors, such as encoders, tachometers, and resolvers. However, the application of actual sensors increases the cost and size of the motor, reduces the reliability of the system, and limits the application in harsh environments [5]. Hence, the PMSM sensorless control strategy is considered a suitable and effective solution, where position and speed information are estimated through electromagnetic information instead of mechanical sensors.

In recent years, many methods have been studied in the literature for sensorless control of PMSM drives [6–10]. Most of the sensorless control technologies are divided into two categories. One is based on the magnetic circuit saturation [11,12], where the position information can be obtained from the response of the injected signal. Due to the requirement of the magnetic saturation-caused saliency, this method can only be applied to the interior permanent-magnet synchronous motor (IPMSM) with the salient polarity.

However, signal processing increases system complexity and is more suitable for low-speed operation [13]. The other is based on back electromotive force (EMF), which extracts the position information from the back-EMF of the motor [14–16]. However, this method cannot be directly applied to IPMSM. Due to the existence of the saliency, the rotor position information of IPMSM is reflected not only in the back-EMF, but also in the inductance. The back-EMF-based method is considered as a suitable sensorless control strategy for the surface permanent magnet synchronous motor (SPMSM), but it is affected by the accuracy of the motor model [17]. The sliding mode observer (SMO) is a nonlinear observer based on the variable structure theory, which reduces the dependence on the system model to some extent [18]. In [19], the sliding mode observer was used to estimate the rotor position, which has good robustness against load disturbance and parameter perturbation. In [20], a full-order sliding mode observer based on synchronous frequency tracking filtering was presented to track the estimated back-EMF harmonics. However, the high-order harmonics in SMO are usually mixed with the back-EMF signals [21]. The low-pass filter (LPF) is needed to extract the fundamental back-EMFs. Nonetheless, the introduction of filters may cause phase delay and complicate the control system, which considerably deteriorates the dynamic performance of PMSM [22]. Another main issue of the traditional SMO is related to chattering caused by discrete-time switching [23]. Several methods have been investigated to weaken the chattering phenomenon. The soft-switching sliding mode observer is suggested to solve the chattering problem of the observer estimation, where the variable boundary layer function is used instead of the traditional switching function [24]. The major drawback of this method is that control input that is too large may lead to saturation of the actuator. In [25], the fast terminal sliding mode for a linear motor positioner is proposed. In this method, the continuous function is employed to approximate the SGN function, which can considerably weaken the chattering issue. Although the system state can be close to the equilibrium point, it will not be achieved in a short time. A similar problem also appears in [26], where the SGN function is substituted with the smooth function of the angle error to weaken the chattering phenomenon. In [27], an improved SMO is applied to obtain rotor position and speed, in which the stator current frequency-variable tracker function is used instead of the switching function to reduce the influence of torque ripple and harmonic components on the back-EMF signals. A nonlinear observer method based on the adaptive sliding mode observer is presented, but the chattering problem still exists with the inclusion of the switching term [28]. In [29], a super-twisting structure was introduced into the design of SMO to estimate rotor position and speed, which uses integral function to eliminate sliding-mode chattering. It can be noted that the aforementioned methods were designed based on the ideal situations without considering the parameter uncertainties, even though the control goals in these methods are achieved. In practical applications, the motor parameters such as resistance and inductance are affected by many factors, resulting in the mismatch between the nominal and actual values. In this case, the estimation accuracy of rotor position and speed is degraded. In [30], a PMSM model with parameter uncertainties is established, in which a high-order sliding mode observer is utilized to reduce chattering and enhance robustness. Nevertheless, the effect in improving the robustness only through the adaptive super-twisting structure is not satisfactory. The accurate position estimation requires exact motor parameters. Generally, disturbance observers are selected by some researchers to provide precise disturbance compensation and improve system performance [31,32]. For instance, in [33], a compound terminal SMO is applied to estimate the parameter disturbances in real time. In [34], an extended sliding mode disturbance observer is designed to observe the system disturbances caused by mismatched parameters and external load, and provide a feed-forward compensation to the controller. However, the introduction of disturbance observers complicates the control system.

Motivated by these problems, an improved super-twisting high-order sliding mode observer is proposed to meet the high-performance sensorless control requirements of SPMSM. The proposed observer is able to simultaneously estimate the rotor position and

speed as well as track system disturbances caused by parameter mismatches in real-time. Moreover, an adaptive observer is integrated to extract the required back-EMF signals, thus improving the estimation accuracy. Finally, simulations and experiments verify the effectiveness of the proposed method. According to the results, the proposed method has a good response performance and precision to ensure the stable operation of the SPMSM system.

The main contributions of this paper are listed as follows:

1. By introducing the super-twisting structure into SMO, the chattering phenomenon and settling time can be reduced.
2. High estimation precision requires accurate motor parameters. Different from the traditional method of applying two observers for PMSM sensorless control with mismatched parameters, only one super-twisting sliding mode observer is designed to simultaneously estimate the rotor position and speed as well as track the parameter disturbances online. In this way, not only is the robustness against the parameter uncertainties enhanced, but the model structure is also simplified.
3. An adaptive observer instead of the low-pass filter and phase compensation module is applied to extract the desired back-EMF signals, so as to further improve the estimation accuracy.

This article is organized as follows. Section 2 describes the improved super-twisting high-order sliding mode observer. Section 3 illustrates and discusses the simulation and experimental results. Some conclusions are drawn in Section 4.

2. Design of the Observer

First, the drive control system structure of PMSM is shown in Figure 1. The control system includes a PMSM, an inverter, a pulse width modulation (PWM) module, two coordinate transformation modules, the PI speed controller, the PI current controller, and the improved super-twisting SMO. The proposed observer is shown in Figure 2. The d -axis reference current i_d^* is usually set to zero to ensure constant flux operating [3]. ω^* is the reference speed. i_q^* is the reference q -axis current. The rotor position and speed estimated by the observer are used for field orientation and closed-loop control. The parameter disturbances estimated by the observer provide the feed-forward compensation terms for the controller after coordinate transformation. In addition, the input of the observer is the given motor voltage recovered from the actually measured dc bus voltage and the duty cycle calculated from the space vector modulation module, which can partially eliminate the dead time effect of the inverter, so as to obtain more accurate actual given motor voltage.

The main work of this paper is to design a back-EMF observer to estimate the rotor position and speed to realize the sensorless speed-tracking control.

2.1. Improved Super-Twisting High-Order Sliding Mode Observer

The dynamics model of the SPMSM in the α - β frame is more convenient for the observer design based on the back-EMF signals. Thus, its mathematical equation considering the model uncertainties can be expressed as follows [30]:

$$\begin{cases} L \frac{di_\alpha}{dt} = -R_s i_\alpha - e_\alpha + u_\alpha + f_\alpha \\ L \frac{di_\beta}{dt} = -R_s i_\beta - e_\beta + u_\beta + f_\beta \end{cases} \quad (1)$$

with

$$\begin{cases} \frac{df_\alpha}{dt} = F_\alpha \\ \frac{df_\beta}{dt} = F_\beta \end{cases} \quad (2)$$

where i_α and i_β are the phase currents in the stationary reference frame, and u_α and u_β are the phase voltages in the stationary reference frame. R_s is the stator resistance. L is the

stator inductance. f_α and f_β represent the uncertainty term vectors, and F_α and F_β are the variation rates of uncertainties f_α and f_β , respectively. The back-EMF signals e_α and e_β are given by the following equation:

$$\begin{cases} e_\alpha = -n_p\omega\Phi \sin \theta \\ e_\beta = n_p\omega\Phi \cos \theta \end{cases} \quad (3)$$

where ω is the mechanical angular speed. θ is the angle of the motor. Φ is the permanent magnet flux. n_p is the number of pole pairs. From (3), it can be seen that the back-EMF signals contain the rotor speed and position information.

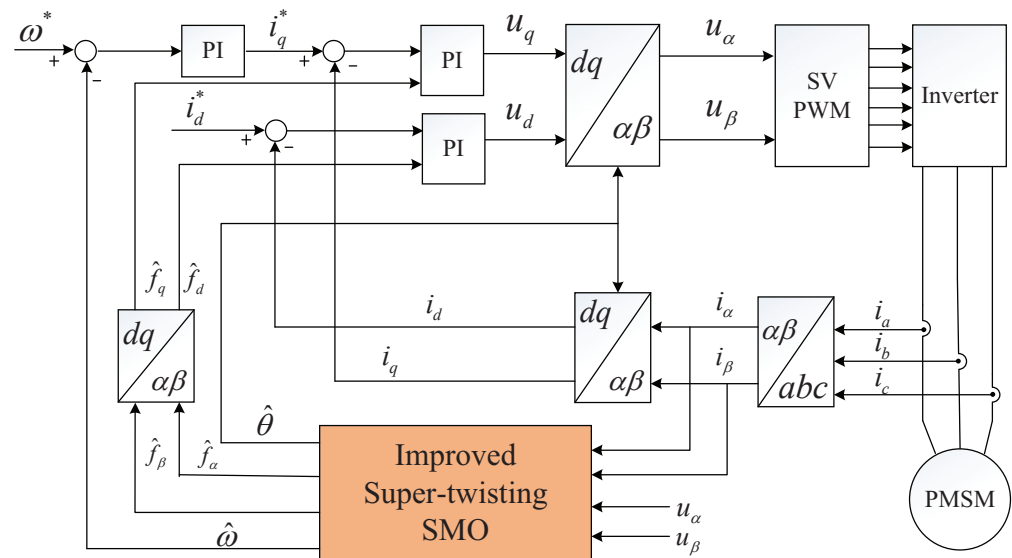


Figure 1. Block diagram of the sensorless control system of PMSM.

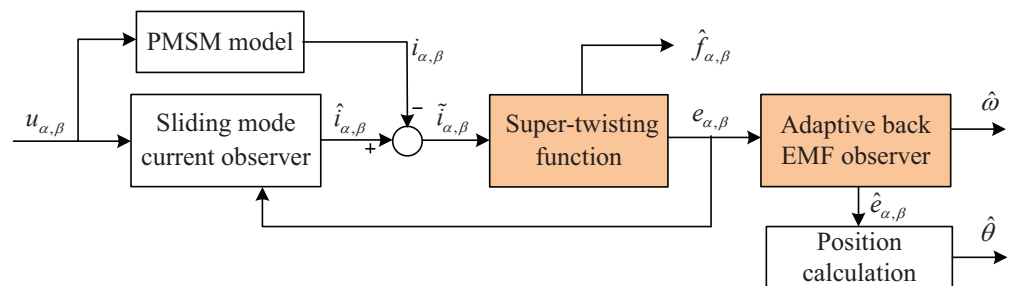


Figure 2. Block diagram of the improved super-twisting SMO.

For the purpose of rotor position estimation and parameter disturbance tracking, the super-twisting high-order sliding mode observer is designed as:

$$\begin{cases} L \frac{d\hat{i}_\alpha}{dt} = -R_s \hat{i}_\alpha + u_\alpha + \hat{f}_\alpha - v_1 \\ \frac{d\hat{f}_\alpha}{dt} = -k_\alpha v_1 \end{cases} \quad (4)$$

$$\begin{cases} L \frac{d\hat{i}_\beta}{dt} = -R_s \hat{i}_\beta + u_\beta + \hat{f}_\beta - v_2 \\ \frac{d\hat{f}_\beta}{dt} = -k_\beta v_2 \end{cases} \quad (5)$$

where \hat{i}_α and \hat{i}_β are the estimations of the phase currents, \hat{f}_α and \hat{f}_β are the estimations of the uncertainties, k_α and k_β are the design parameters, and v_1 and v_2 represent the observer control functions.

The SMO with a super-twisting algorithm can effectively weaken system chattering and shorten the tracking time, which is defined as:

$$\begin{bmatrix} v_1 \\ v_2 \end{bmatrix} = \begin{bmatrix} k_1 |\tilde{i}_\alpha|^{1/2} \text{sgn}(\tilde{i}_\alpha) + \int k_2 \text{sgn}(\tilde{i}_\alpha) dt \\ k_1 |\tilde{i}_\beta|^{1/2} \text{sgn}(\tilde{i}_\beta) + \int k_2 \text{sgn}(\tilde{i}_\beta) dt \end{bmatrix} \quad (6)$$

where k_1 and k_2 are sliding-mode gains, $k_1 > 0$ and $k_2 > 0$.

According to (1), (2), (4), and (5), the error equation can be obtained as:

$$\begin{cases} L \frac{d\tilde{i}_\alpha}{dt} = -R_s \tilde{i}_\alpha + e_\alpha + \tilde{f}_\alpha - v_1 \\ \frac{d\tilde{f}_\alpha}{dt} = -k_\alpha v_1 - F_\alpha \end{cases} \quad (7)$$

$$\begin{cases} L \frac{d\tilde{i}_\beta}{dt} = -R_s \tilde{i}_\beta + e_\beta + \tilde{f}_\beta - v_2 \\ \frac{d\tilde{f}_\beta}{dt} = -k_\beta v_2 - F_\beta \end{cases} \quad (8)$$

where $\tilde{i}_\alpha = \hat{i}_\alpha - i_\alpha$ and $\tilde{i}_\beta = \hat{i}_\beta - i_\beta$ are the current estimation errors, and $\tilde{f}_\alpha = \hat{f}_\alpha - f_\alpha$ and $\tilde{f}_\beta = \hat{f}_\beta - f_\beta$ are the uncertainties' estimation errors.

The estimation errors of stator currents are selected to construct the sliding surface as:

$$s = [\tilde{i}_\alpha \quad \tilde{i}_\beta]^T \quad (9)$$

The first derivative of the sliding surface is:

$$\begin{cases} \dot{\tilde{i}}_\alpha = \frac{1}{L} \left(-k_1 |\tilde{i}_\alpha|^{1/2} \text{sgn}(\tilde{i}_\alpha) - \int k_2 \text{sgn}(\tilde{i}_\alpha) dt \right) + D_1 \\ D_1 = \frac{R}{L} \tilde{i}_\alpha + \frac{1}{L} e_\alpha + \frac{1}{L} \tilde{f}_\alpha \\ \dot{\tilde{i}}_\beta = \frac{1}{L} \left(-k_1 |\tilde{i}_\beta|^{1/2} \text{sgn}(\tilde{i}_\beta) - \int k_2 \text{sgn}(\tilde{i}_\beta) dt \right) + D_2 \\ D_2 = \frac{R}{L} \tilde{i}_\beta + \frac{1}{L} e_\beta + \frac{1}{L} \tilde{f}_\beta \end{cases} \quad (10)$$

Compared with the standard form of the super-twisting algorithm [35], it is found that D_1 and D_2 are considered as the disturbance terms of the observer. Once the system reaches the sliding surface, $\tilde{i}_\alpha = \tilde{i}_\beta = 0$ and $\dot{\tilde{i}}_\alpha = \dot{\tilde{i}}_\beta = 0$, the estimated back-EMF signals can be expressed as:

$$\begin{cases} e_\alpha = k_1 |\tilde{i}_\alpha|^{1/2} \text{sgn}(\tilde{i}_\alpha) + \int k_2 \text{sgn}(\tilde{i}_\alpha) dt \\ e_\beta = k_1 |\tilde{i}_\beta|^{1/2} \text{sgn}(\tilde{i}_\beta) + \int k_2 \text{sgn}(\tilde{i}_\beta) dt \end{cases} \quad (11)$$

According to (11), the back-EMF equivalent signals can be obtained, but the estimated signals still contain high-frequency components. An adaptive observer instead of the traditional low-pass filter is applied to extract the required back-EMF signals. Since the change rate of the motor angular velocity is much lower than that of the stator current, we can assume that $\dot{\omega} = 0$. Then, the back-EMFs model of the PMSM can be expressed as [26]:

$$\begin{cases} \frac{de_\alpha}{dt} = -n_p \omega e_\beta \\ \frac{de_\beta}{dt} = n_p \omega e_\alpha \end{cases} \quad (12)$$

Based on (12), the adaptive observer is constructed as:

$$\begin{cases} \frac{d\hat{e}_\alpha}{dt} = -n_p \hat{\omega} \hat{e}_\beta - k_3 (\hat{e}_\alpha - e_\alpha) \\ \frac{d\hat{e}_\beta}{dt} = n_p \hat{\omega} \hat{e}_\alpha - k_4 (\hat{e}_\beta - e_\beta) \\ \frac{d\hat{\omega}}{dt} = \frac{1}{n_p} [(\hat{e}_\alpha - e_\alpha) \hat{e}_\beta - (\hat{e}_\beta - e_\beta) \hat{e}_\alpha] \end{cases} \quad (13)$$

where k_3 and k_4 are the observer gains, $k_3 > 0$ and $k_4 > 0$.

The error equation of the adaptive observer is derived by subtracting (12) from (13):

$$\begin{cases} \frac{d\tilde{e}_\alpha}{dt} = -n_p\tilde{\omega}\tilde{e}_\beta - n_p\omega\tilde{e}_\beta - k_3\tilde{e}_\alpha \\ \frac{d\tilde{e}_\beta}{dt} = n_p\tilde{\omega}\tilde{e}_\alpha + n_p\omega\tilde{e}_\alpha - k_4\tilde{e}_\beta \\ \frac{d\tilde{\omega}}{dt} = \frac{1}{n_p}[\tilde{e}_\alpha\tilde{e}_\beta - \tilde{e}_\beta\tilde{e}_\alpha] \end{cases} \quad (14)$$

where $\tilde{e}_\alpha = \hat{e}_\alpha - e_\alpha$ and $\tilde{e}_\beta = \hat{e}_\beta - e_\beta$ are the back-EMF estimation errors, and $\tilde{\omega} = \hat{\omega} - \omega$ are the speed estimation errors.

According to (13), the rotor position can be calculated from the relationship between the back-EMF and the rotor position.

$$\hat{\theta} = \arctan\left(-\frac{\hat{e}_\alpha}{\hat{e}_\beta}\right) \quad (15)$$

2.2. Observer Stability Analysis

According to the Lyapunov stability theorem, the sliding mode system is stable if:

1. $t \rightarrow \infty, s \rightarrow 0$;
2. $s\dot{s} < 0$.

A Lyapunov function is selected to ensure that all trajectories of the system converge to the origin in finite time [35].

$$\begin{aligned} V &= \frac{1}{2}V_\alpha(\tilde{i}_\alpha) + \frac{1}{2}V_\beta(\tilde{i}_\beta) \\ &= 2k_2|\tilde{i}_\alpha| + \frac{1}{2}\zeta_\alpha^2 + \frac{1}{2}\left(k_1|\tilde{i}_\alpha|^{1/2}\text{sgn}(\tilde{i}_\alpha) - \zeta_\alpha\right)^2 \\ &\quad + 2k_2|\tilde{i}_\beta| + \frac{1}{2}\zeta_\beta^2 + \frac{1}{2}\left(k_1|\tilde{i}_\beta|^{1/2}\text{sgn}(\tilde{i}_\beta) - \zeta_\beta\right)^2 \end{aligned} \quad (16)$$

Since $\tilde{i}_\alpha = \tilde{i}_\beta = 0$ is an equilibrium point of the super-twisting function, the proposed Lyapunov function can be written in quadratic form $V(x) = A^T P A + B^T P B$, where

$$\begin{aligned} [A \quad B] &= \begin{bmatrix} |\tilde{i}_\alpha|^{1/2}\text{sgn}(\tilde{i}_\alpha) & |\tilde{i}_\beta|^{1/2}\text{sgn}(\tilde{i}_\beta) \\ \zeta_\alpha & \zeta_\beta \end{bmatrix} \\ P &= \begin{bmatrix} \frac{-4k_2+k_1^2}{2} & -\frac{k_1}{2} \\ -\frac{k_1}{2} & 1 \end{bmatrix} \\ [\zeta_\alpha \quad \zeta_\beta] &= [-\int k_2\text{sgn}(\tilde{i}_\alpha)dt \quad -\int k_2\text{sgn}(\tilde{i}_\beta)dt] \end{aligned} \quad (17)$$

Note that $V(x)$ is a strong Lyapunov function which is continuous everywhere but non-differentiable at $\tilde{i}_\alpha = \tilde{i}_\beta = 0$.

Suppose that D_1 and D_2 are globally bounded by:

$$D_1 \leq \sigma|\tilde{i}_\alpha|^{1/2} \quad (18)$$

$$D_2 \leq \sigma|\tilde{i}_\beta|^{1/2} \quad (19)$$

for any constants $\sigma \geq 0$. Then, the convergence of all trajectories in finite time can be guaranteed when the gains are properly selected.

By taking the time-derivative of (16), we get:

$$\dot{V} = -\frac{1}{2}k_1|\tilde{i}_\alpha|^{-1/2}A^T P A - \frac{1}{2}k_1|\tilde{i}_\beta|^{-1/2}B^T P B \quad (20)$$

where

$$P = \frac{k_1}{2} \begin{bmatrix} 2k_2 + k_1^2 & -k_1 \\ -k_1 & 1 \end{bmatrix} \quad (21)$$

$\dot{V}(x)$ is negative-definite if:

$$\begin{cases} k_1 > 2\sigma \\ k_2 > k_1 \frac{5\sigma k_1 + 4\sigma^2}{2(k_1 - 2\sigma)} \end{cases} \quad (22)$$

Hence, the global asymptotic stability of the proposed observer can be proved by using the Lyapunov stability theory. Moreover, the sliding chattering is effectively weakened since the sign function is hidden in the integral term.

3. Simulation and Experimental Results

3.1. Simulation Results

In order to demonstrate the effectiveness of the proposed observer, the simulation model based on a sensorless SPMSM drive system is built in MATLAB/Simulink, where the motor position and speed information are obtained from the proposed observer. Moreover, the mechanical sensor is applied to record the actual position and speed for comparison. The motor parameters are listed in Table 1. The observer parameters are set as $k_1 = 500$, $k_2 = 0.1$, $k_\alpha = 10$, $k_\beta = 10$, $k_3 = k_4 = 170$.

Table 1. PMSM parameters.

Description	Value	Unit
rated speed	1000	r/min
rated torque	10	N·m
stator resistance	0.93	Ω
d -and q -axis inductance	3	mH
permanent magnet flux	0.32	Wb
moment of inertia	0.0027	kg·m ²

Figure 3 shows the simulation waveform of the proposed observer, and the load torque is 5 Nm. The speed response is given in Figure 3a. As depicted, it takes very little time for the actual speed to be adjusted to the reference speed. The estimated speed is closely related to the actual speed, and the estimated error quickly converges to zero after the short transient period, as shown in Figure 3b. The maximum dynamic error of the estimated speed is 5 rpm and the steady-state error is within 0.1 rpm. In Figure 3c, two quadrature smooth estimated back-EMFs are obtained. Figure 3d displays the electrical position response, which shows an excellent estimation performance with the proposed observer. The position estimation error is given in Figure 3e. Figure 3 indicates that the proposed observer can effectively estimate the speed and position and track the reference signal well.

Figure 4a shows the speed response with the load torque stepped from 5 Nm to 10 Nm at 1 s. As shown, the estimated speed keeps a close track with the actual value. After the step load occurs, the estimated speed quickly returns to the reference, and the steady-state error increases from 0.1 rpm to 0.4 rpm. The robustness of the proposed observer is verified. The three-phase current response is presented in Figure 4b.

Since it is inevitable that the motor parameters vary with the operating conditions, the influence of parameter deviations is considered. The speed response and disturbance estimation results under different parameter mismatches are presented in Figures 5–10. The load torque is 5 Nm. Figures 5 and 6 respectively show the speed response and estimation error with different stator inductance values. In Figure 5, when the inductance increases from L to $2L$, the adjustment time increases by 0.04 s, and the steady-state fluctuation values of f_d and f_q are 4 V and 0.4 V, respectively. In Figure 6, when the inductance is

reduced from L to $0.5L$, an overshoot of about 2 rad occurs, and the fluctuations of f_d and f_q are 3 V and 0.6 V, respectively.

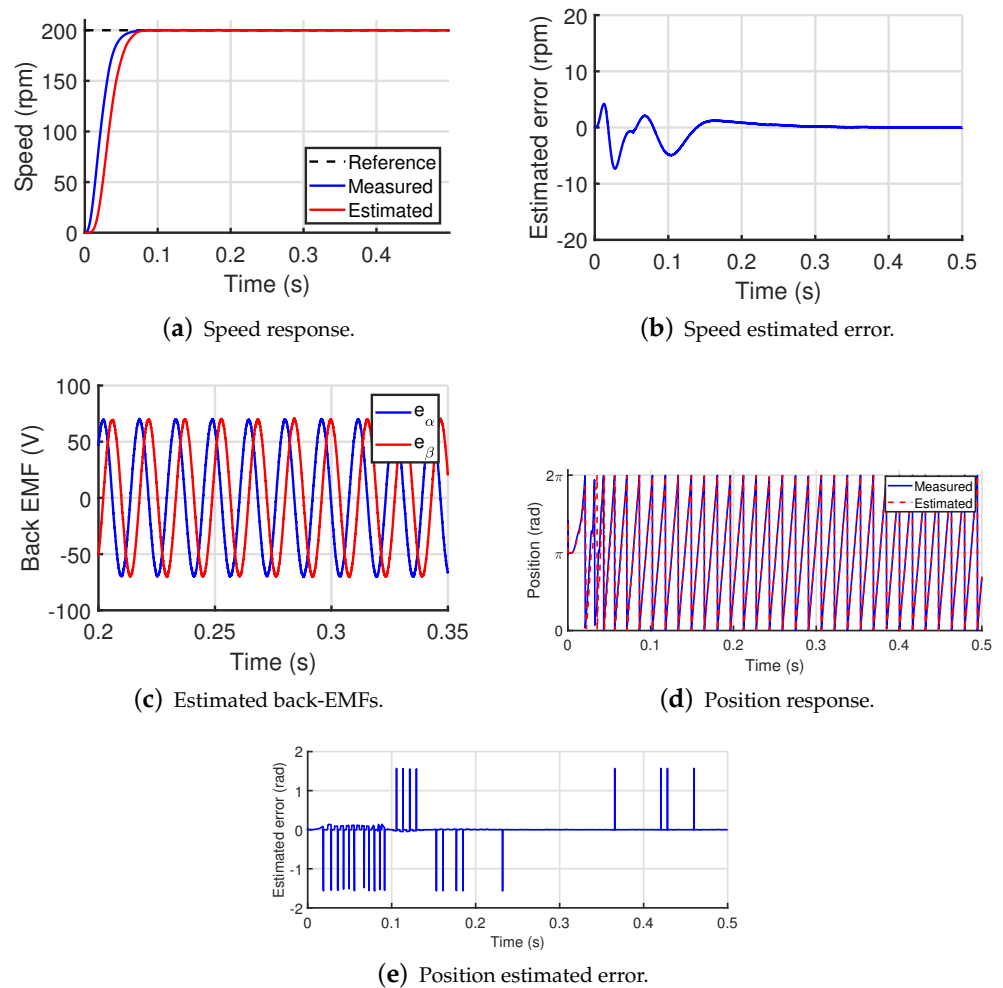


Figure 3. Simulation results of the proposed observer under nominal parameters.

Figures 7 and 8 respectively show the speed response and estimation error with different resistance values. The fluctuations in the estimated speed and the estimated disturbance are much increased compared to other parameter-mismatched situations, especially when the resistance increases, where the f_d and f_q rise to 10 V and 5 V, respectively. The speed estimates and disturbance estimates when the stator inductance and resistance change simultaneously are given in Figures 9 and 10. From these Figures, it can be observed that the proposed observer can still track the reference signal quickly and accurately even if the parameters are mismatched.

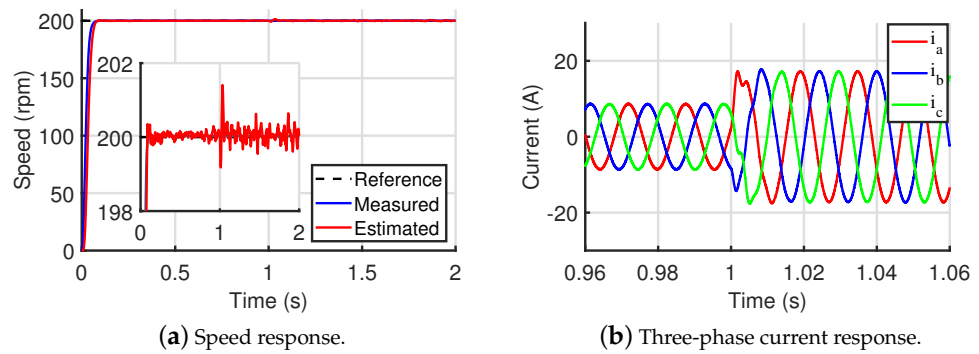


Figure 4. Simulation results of the proposed observer with stepped load.

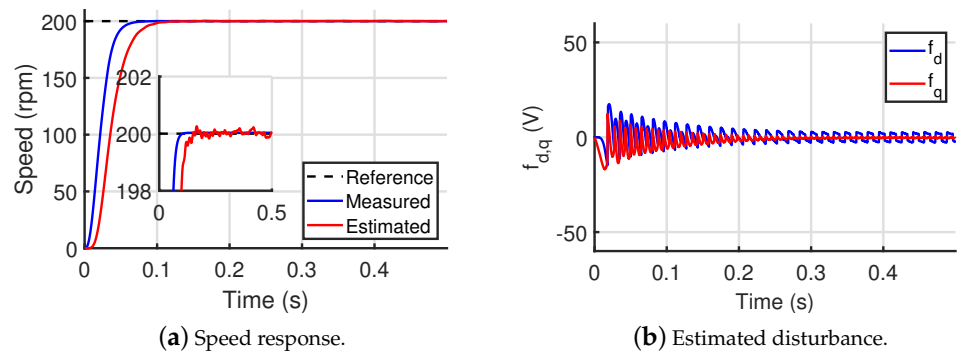


Figure 5. Simulation results under $L = 2L_0$.

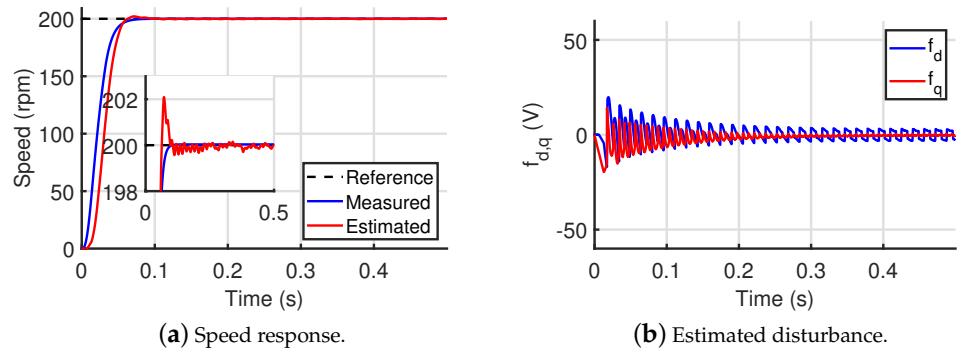


Figure 6. Simulation results under $L = 0.5L_0$.

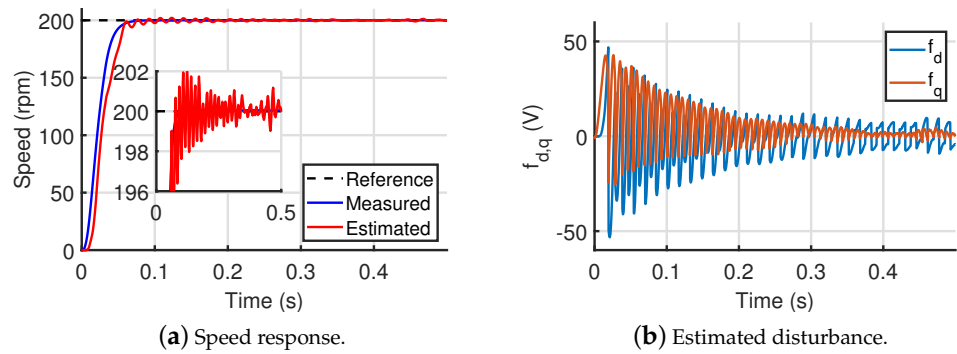


Figure 7. Simulation results under $R = 10R_0$.

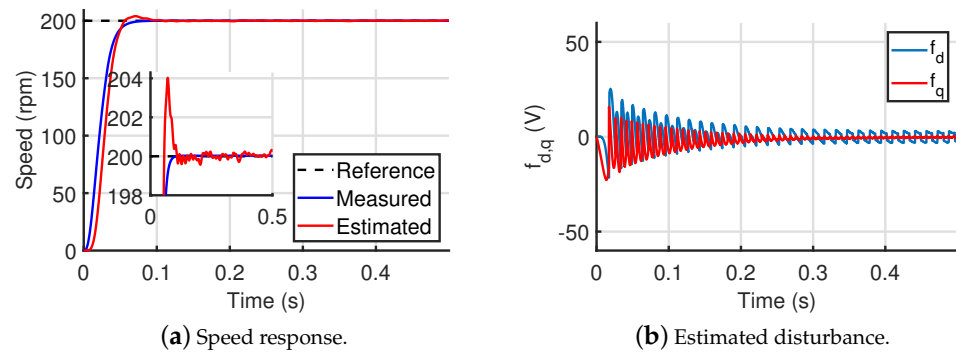


Figure 8. Simulation results under $R = 0.1R_0$.

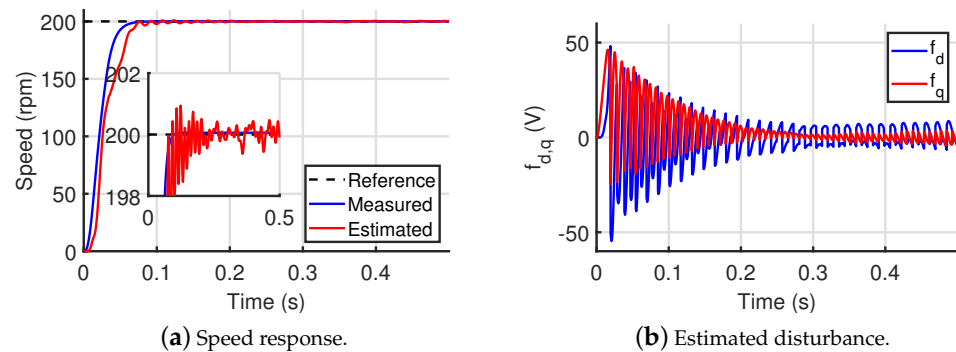


Figure 9. Simulation results under $L = 2L_0, R = 10R_0$.

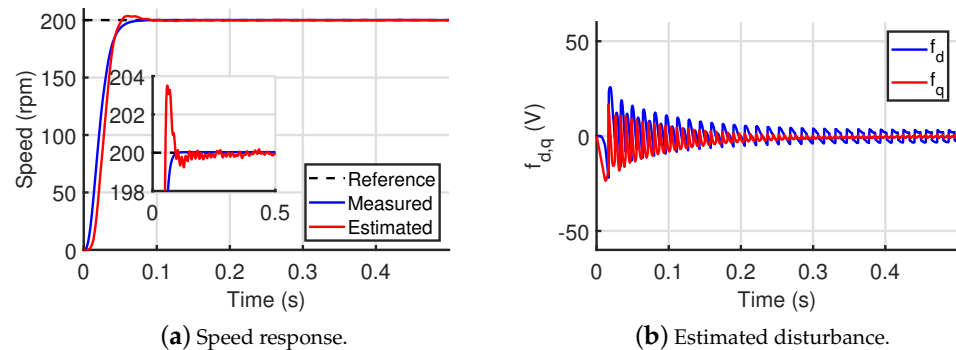


Figure 10. Simulation results under $L = 0.5L_0, R = 0.1R_0$.

3.2. Experimental Results

The experimental results were obtained using the AC servo system rapid prototyping experimental platform. The experimental platform diagram is given in Figure 11. The platform consists of hardware and software. The hardware includes the servo motor, real-time simulator, and torque sensor. Software includes MATLAB/Simulink and RT-SIM. The platform uses MATLAB/Simulink to build and compile the model of the control system, then download it to the simulator to drive the motor. The real-time transmission of the data and signal can be realized by using RT-SIM. The configuration of the experimental system is shown in Figure 12.

A sensstrol 130MB150A type SPMSM is applied in the experiment. All the parameters in the experiment are consistent with the simulation. The sampling interval is 0.0002 s and the PWM sampling frequency is 10 kHz. It should be emphasized again that the use of a mechanical sensor in the experiment is only to record the actual position and speed for comparison.

The proposed observer is compared with the other two observers, and the traditional SMO and the traditional super-twisting algorithm (STA) as presented in [30]. The

experimental results investigate the dynamic and steady-state performance of the proposed observer. Figures 13–26 show the estimated speed and estimation error in different speed ranges.

Figures 13–15 illustrate the experimental results of three observers from zero speed to high speed (1000 rpm). The estimated speed of the three observers is basically consistent with the actual speed. In Figure 13, with the traditional SMO, the estimated speed quickly tracks the actual speed in the transient state, whereas serious chattering occurs in the steady state. As shown in Figure 14, the traditional STA-based observer has lower steady-state estimation error since the super-twisting structure provides accurate speed estimation and weakens sliding chattering. However, more adjustment time is needed for PMSM to reach the steady state. In Figure 15, the proposed observer could reduce transient and steady-state errors and provide better estimation accuracy, which can be confirmed by comparing the estimation errors in Figures 13b, 14b and 15b. It indicates that the proposed observer has faster convergence speed and minimal error compared to the other two observers.

The motor speed response and estimated error from zero speed to medium speed (600 rpm) are presented in Figures 16–18. In Figure 16, the traditional SMO has overshoot and fluctuation. In Figure 17, by applying the super-twisting algorithm, the chattering caused by repeated overshoot is reduced, but the dynamic estimation performance is compromised to some extent. In Figure 18, the estimated speed converges quickly to the actual value. It can be seen from the steady-state error in Figures 16b, 17b, and 18b that the proposed observer has better estimation accuracy compared with the other two observers.

The low-speed estimation result is given in Figures 19–21, where the speed changes from 60 rpm to 30 rpm. In Figure 19, significant fluctuation appears with the traditional SMO. In Figure 20, the issue is improved by the super-twisting algorithm, but the distinct estimated adjustment period and dynamic estimation error appears after the speed is changed. It can be seen from Figure 21 that the speed estimation error of the proposed observer has been drastically reduced. Compared with the other two observers, the proposed observer still maintains good estimation accuracy in the process of speed change, which can be proved from the estimation error in Figures 19b, 20b, and 21b.

Then, the speed estimation performance under a variable speed reference profile (industrial benchmark) is evaluated. The test can be regarded as including all the previous experimental tests. Figures 22–24 show the speed estimation and estimation errors of all observers from zero to medium speed (400 rpm) to high speed (1000 rpm) and then to medium-high speed (700 rpm). It can be observed from Figure 22 that the traditional SMO shows high error and unacceptable overshoot. The super-twisting structure could eliminate this phenomenon, but more regulation time is required in the transient one, as shown in Figure 23. In Figure 24, the smaller estimation error in the steady state and the fast convergence speed in the transient state are provided by the proposed observer. Figure 25 shows the position estimation performance of the proposed observer when the speed steps at 8 s from 400 rpm to 1000 rpm. The position maintains a good position performance even if the speed is changed. Thus, the proposed observer gets the best speed estimation during the change of speed reference. The quantitative comparison of the three observers is shown in Table 2.

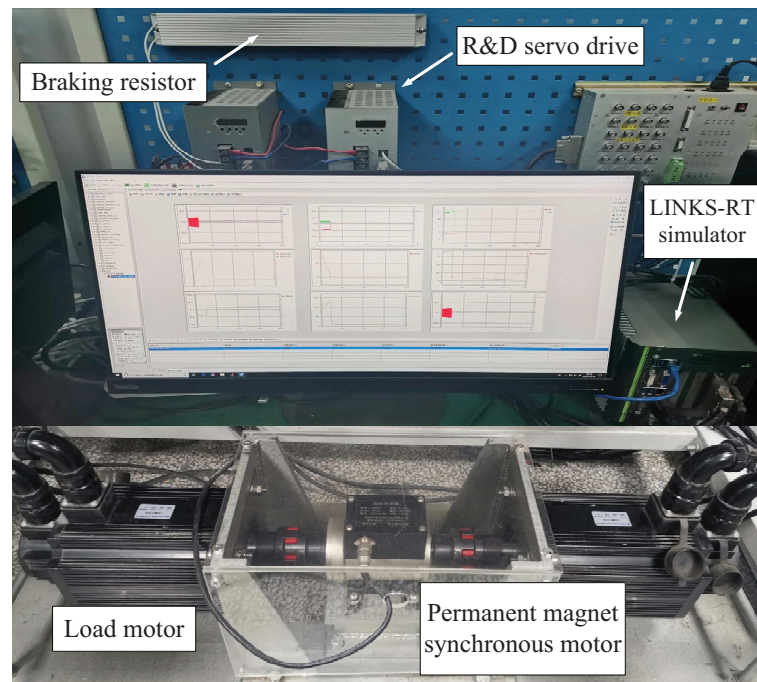


Figure 11. Experimental configuration of PMSM system.

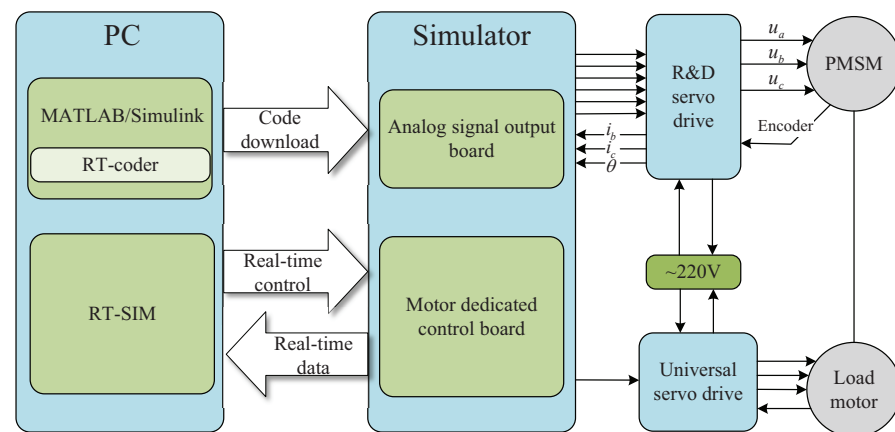


Figure 12. Experimental configuration of PMSM system.

The feasibility experiment in the high-speed and stepped load is carried out, and the result is shown in Figure 26. The motor operates in 1000 rpm with the load stepped from 2 N to 4 N at 1 s. Figure 26a gives the measured and estimated speeds, which shows that the actual speed quickly returns to the reference speed after load torque-stepping. The estimated speed is still close to the measured speed. The position maintains a good estimation performance both in the dynamic and steady state, as shown in Figure 26b.

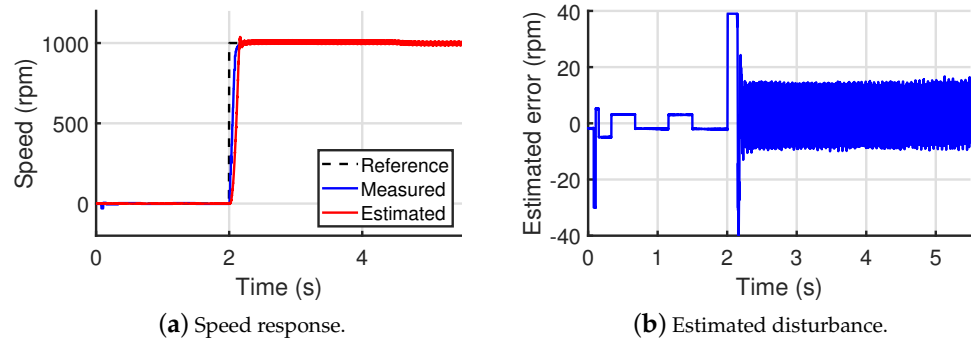


Figure 13. Experimental results of SMO at 1000 rpm.

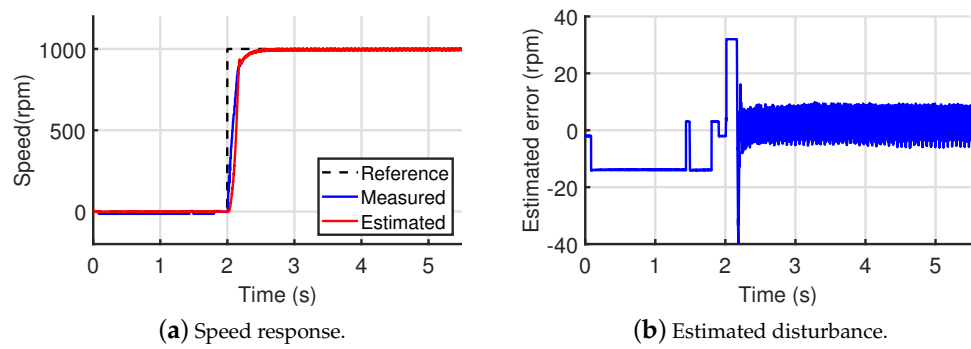


Figure 14. Experimental results of STA at 1000 rpm.

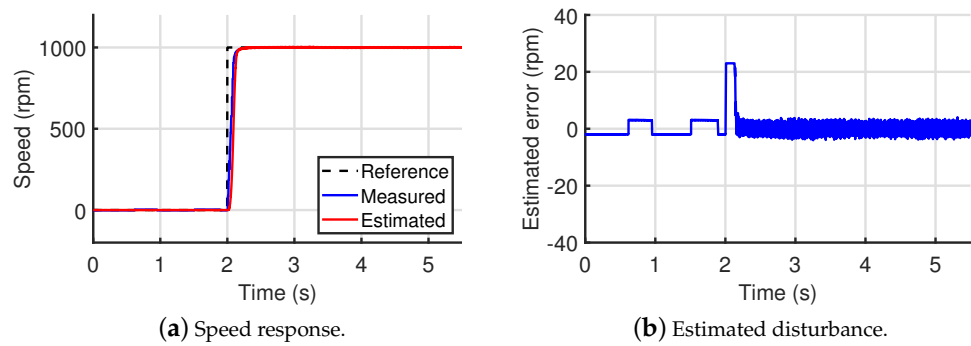


Figure 15. Experimental results of the proposed observer at 1000 rpm.

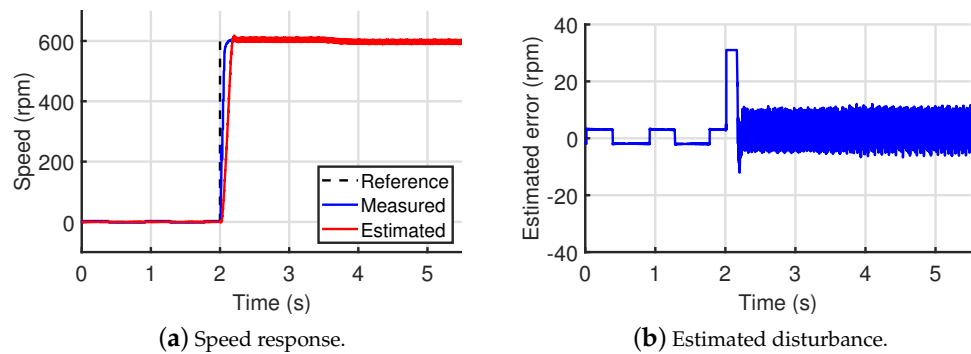


Figure 16. Experimental results of SMO at 600 rpm.

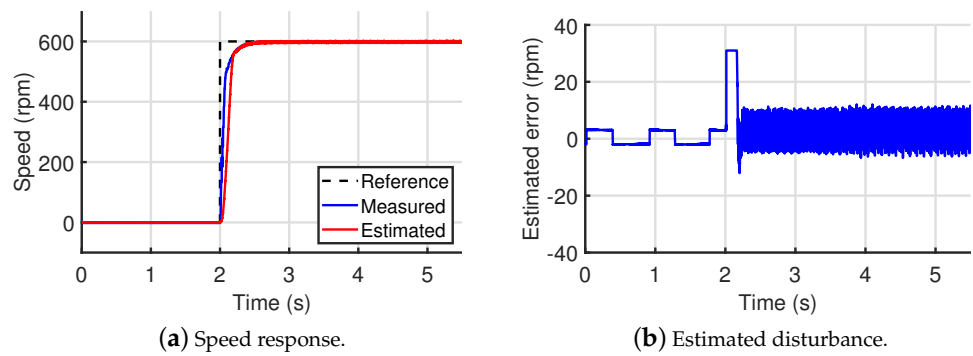


Figure 17. Experimental results of STA at 600 rpm.

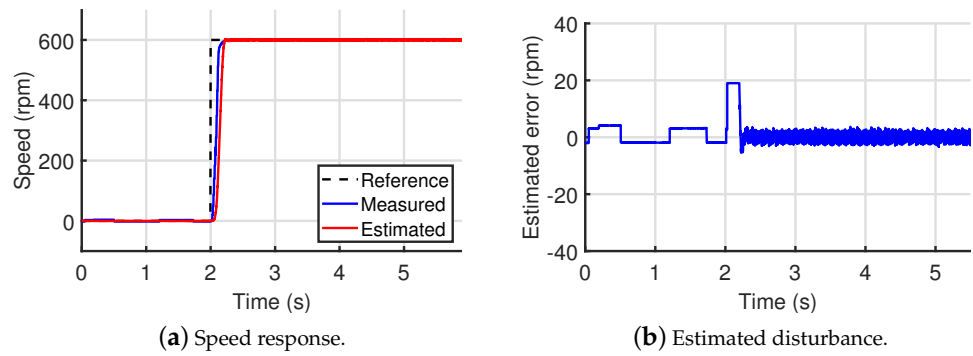


Figure 18. Experimental results of the proposed observer at 600 rpm.

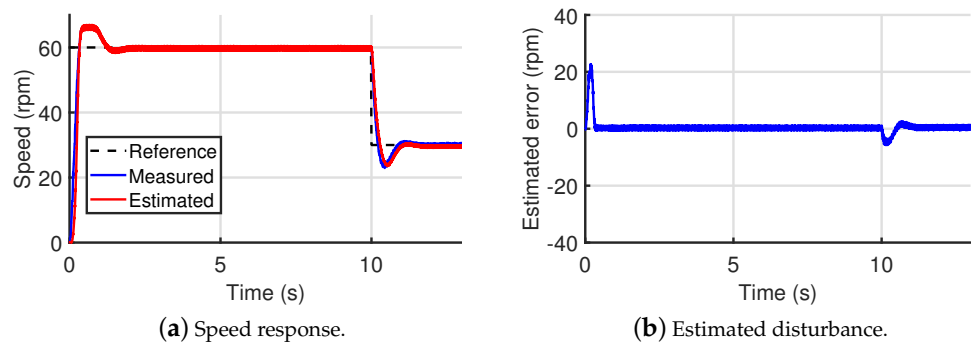


Figure 19. Experimental results of SMO under 60 rpm to 30 rpm.

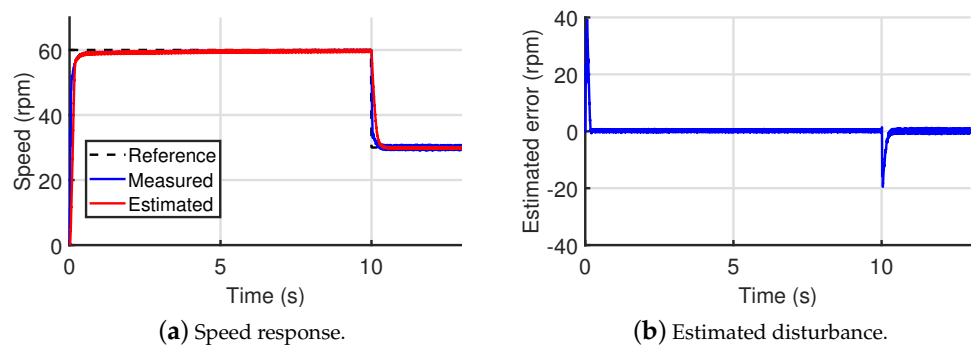


Figure 20. Experimental results of STA under 60 rpm to 30 rpm.

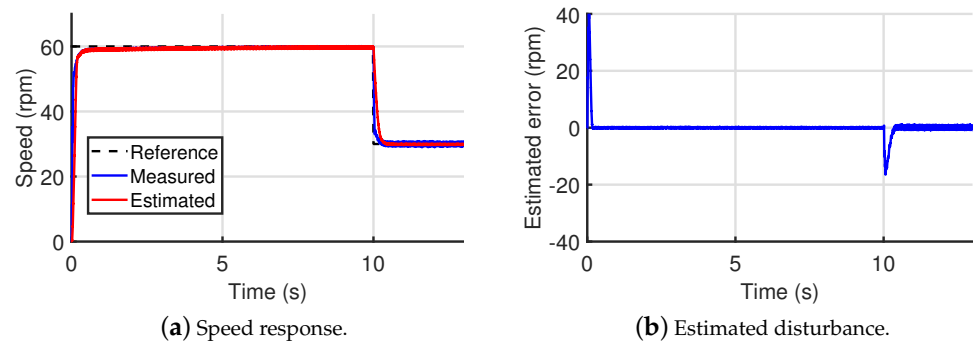


Figure 21. Experimental results of the proposed observer under 60 rpm to 30 rpm.

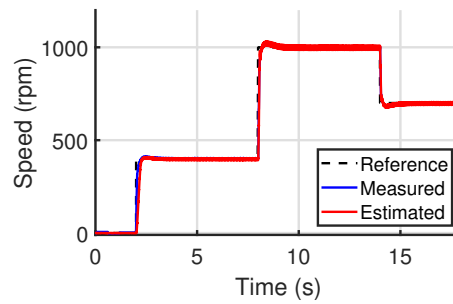


Figure 22. Experimental results of SMO at variable speed.

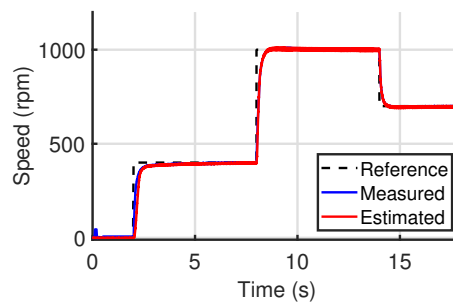


Figure 23. Experimental results of STA at variable speed.

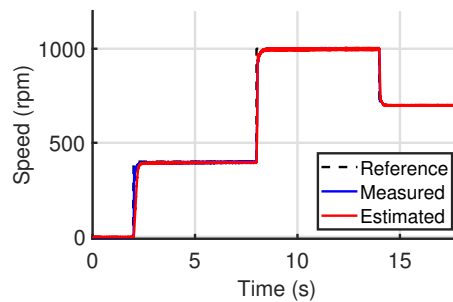


Figure 24. Experimental results of the proposed observer at variable speed.

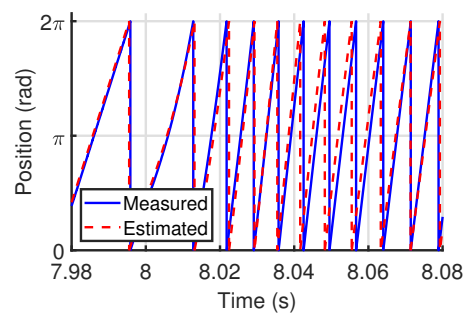


Figure 25. Position magnification under variable speed.

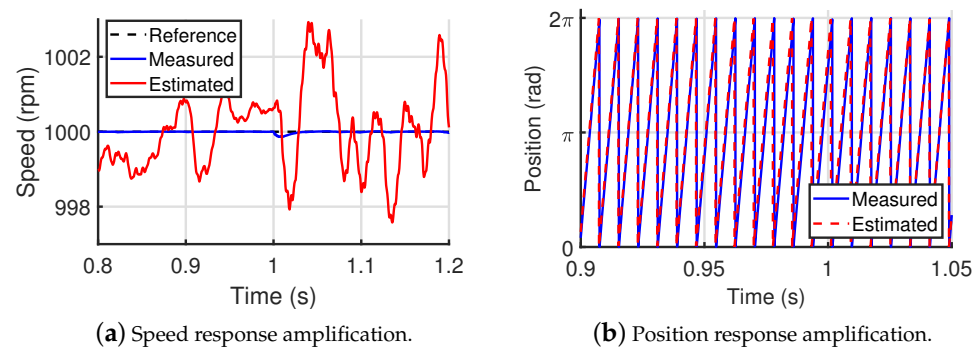


Figure 26. Experimental results under stepped load.

Table 2. Comparison analysis of experimental results.

Speed	Method	Steady-State Error	Tracking Time	Estimated Time
1000 rpm	traditional SMO	10 rpm	2.19 s	2.22 s
	traditional STA	7 rpm	2.55 s	2.56 s
	proposed observer	4 rpm	2.20 s	2.20 s
600 rpm	traditional SMO	9 rpm	2.23 s	2.25 s
	traditional STA	5 rpm	2.51 s	2.52 s
	proposed observer	3 rpm	2.22 s	2.22 s
60 → 30 rpm	traditional SMO	1 rpm	0.9 s	1 s
	traditional STA	0.8 rpm	0.3 s	0.5 s
	proposed observer	0.5 rpm	0.3 s	0.4 s

Tracking time refers to the time taken for the measured position to reach the reference position. Estimated time refers to the time taken for the estimated position to reach the reference position.

4. Conclusions

In this article, an improved super-twisting sliding mode observer was presented for the sensorless control of the SPMSM system. The purpose of the proposed observer was to accurately estimate the rotor position and speed. The main idea is to use only one observer to simultaneously estimate the rotor position and speed, as well as track the parameter perturbation in real time. The robustness and estimation accuracy of the system can be ensured even under the influence of parameter uncertainties. Moreover, both good dynamic and steady-state performance can be achieved. The simulation results show that the proposed method performs well for nominal or uncertain parameters. The advantages and benefits of this method in sensorless speed-tracking were verified by comparative experiments. Therefore, the effectiveness and feasibility of the method proposed in this paper in practical engineering can be guaranteed.

Although the proposed method maintains a correct estimation at zero speed, its steady-state error and overshoot increases to some extent. In future research work, we plan to design a sensorless control scheme which can realize high-performance operation in a full speed range by combining the respective advantages of the magnetic circuit saturation-based method and back-EMF-based method.

Author Contributions: Y.Z. conceived and wrote the paper; S.W. contributed analysis tools; H.Y. proposed the theory. All authors have read and agreed to the published version of the manuscript.

Funding: This work was funded by the National Natural Science Foundation of China under Grant 61573203.

Institutional Review Board Statement: Not Applicable.

Informed Consent Statement: Not Applicable.

Data Availability Statement: Not Applicable.

Acknowledgments: The authors also thank Herong Wu for support of the experimental equipment.

Conflicts of Interest: The authors declare no conflict of interest.

Abbreviations

The following abbreviations are used in this manuscript:

PMSM	Permanent Magnet Synchronous Motor
IPMSM	Interior Permanent Magnet Synchronous Motor
SPMSM	surface permanent magnet synchronous motor
EMF	Electromotive Force
SMO	Sliding Mode Observer
LPF	Low Pass Filter
HSMO	High-order Sliding Mode Observer
STA	Super Twisting Algorithm

References

1. Tan, L.N.; Cong, T.P.; Cong, D.P. Neural network observers and sensorless robust optimal control for partially unknown PMSM with disturbances and saturating voltages. *IEEE Trans. Power Electron.* **2021**, *36*, 12045–12056. [[CrossRef](#)]
2. Sun, X.; Yu, H.; Yu, J.; Liu, X. Design and implementation of a novel adaptive backstepping control scheme for a PMSM with unknown load torque. *IET Electr. Power Appl.* **2019**, *13*, 445–455. [[CrossRef](#)]
3. Liu, X.; Yu, H.; Yu, J.; Lin, Z. Combined speed and current terminal sliding mode control with nonlinear disturbance observer for PMSM drive. *IEEE Access* **2018**, *6*, 29594–29601. [[CrossRef](#)]
4. Liu, A.; Yu, H. Smooth-switching control of robot-based permanent-magnet synchronous motors via port-controlled Hamiltonian and feedback linearization. *Energies* **2020**, *13*, 5731. [[CrossRef](#)]
5. Zhao, W.; Jiao, S.; Chen, Q.; Xu, D.; Ji, J. Sensorless control of a linear permanent-magnet motor based on an improved disturbance observer. *IEEE Trans. Ind. Electron.* **2018**, *65*, 9291–9300. [[CrossRef](#)]
6. Chen, S. Design and performance analysis of an iterative flux sliding-mode observer for the sensorless control of PMSM drives. *ISA Trans.* **2019**, *94*, 255–264.
7. Xiao, D.; Nalakath, S.; Filho, S.R.; Fang, G.; Emadi, A. Universal full-speed sensorless control scheme for interior permanent magnet synchronous motors. *IEEE Trans. Power Electron.* **2021**, *36*, 4723–4737. [[CrossRef](#)]
8. Luo, X.; Shen, A.; Tang, Q.; Liu, J.; Xu, J. Two-step continuous-control set model predictive current control strategy for SPMSM sensorless drives. *IEEE Trans. Energy Convers.* **2021**, *36*, 1110–1120. [[CrossRef](#)]
9. Reigosa, D.; Ye, G.K.; Martinez, M.; Fernandez, D.; Briz, F. Sensorless control of wound rotor synchronous motors based on rotor high-frequency signal injection. *IEEE Trans. Ind. Appl.* **2021**. [[CrossRef](#)]
10. Repecho, V.; Waqar, J.; Biel, D.; Doria-Cerezo, A. Zero speed sensorless scheme for PMSM under decoupled sliding mode control. *IEEE Trans. Ind. Electron.* **2021**, *31*. [[CrossRef](#)]
11. Lee, J.; Kwon, Y.C.; Sul, S.K. Signal-injection sensorless control with tilted current reference for heavily saturated IPMSMs. *IEEE Trans. Power Electron.* **2020**, *35*, 12100–12109. [[CrossRef](#)]
12. Accetta, A.; Cirrincione, M.; Pucci, M.; Vitale, G. Sensorless control of PMSM fractional horsepower drives by signal injection and neural adaptive-band filtering. *IEEE Trans. Ind. Electron.* **2011**, *59*, 1355–1366. [[CrossRef](#)]
13. Li, H.; Zhang, X.; Yang, S.; Liu, S. Unified graphical model of high-frequency signal injection methods for PMSM sensorless control. *IEEE Trans. Ind. Electron.* **2020**, *67*, 4411–4421. [[CrossRef](#)]
14. Xu, W.; Jiang, Y.; Mu, C.; Blaabjerg, F. Improved nonlinear flux observer based second-order SOIFO for PMSM sensorless control. *IEEE Trans. Power Electron.* **2019**, *34*, 565–579. [[CrossRef](#)]
15. Li, L.; Zhang, Z.; Wang, C. A flexible current tracking control of sensorless induction motors via adaptive observer. *ISA Trans.* **2019**, *93*, 180–188. [[CrossRef](#)]
16. Ge, Y.; Yang, L.; Ma, X. Sensorless control of PMSM using generalized extended state observer and adaptive resistance estimation. *IET Electr. Power Appl.* **2020**, *14*, 2062–2073. [[CrossRef](#)]

17. Lu, W.; Tang, B.; Ji, K.; Lu, K.; Yu, Z. A new load adaptive identification method based on an improved sliding mode observer for PMSM position servo system. *Energies* **2021**, *36*, 3211. [[CrossRef](#)]
18. Chen, S.; Zhang, X.; Wu, X.; Tan, G.; Chen, X. Sensorless control for IPMSM based on adaptive super-twisting sliding-mode observer and improved phase-locked loop. *IEEE Trans. Power Electron.* **2019**, *12*, 1225. [[CrossRef](#)]
19. Wang, M.S.; Tsai, T. Sliding mode and neural network control of sensorless PMSM controlled system for power consumption and performance improvement. *Energies* **2017**, *10*, 1780. [[CrossRef](#)]
20. Bao, D.; Wu, H.; Wang, R.; Zhao, F.; Pan, X. Full-order sliding mode observer based on synchronous frequency tracking filter for high-speed interior PMSM sensorless drives. *Energies* **2020**, *13*, 6511. [[CrossRef](#)]
21. Zaky, M.S.; Metwally, M.K.; Azazi, H.; Deraz, S. A new adaptive SMO for speed estimation of sensorless induction motor drives at zero and very low frequencies. *IEEE Trans. Ind. Electron.* **2018**, *65*, 6901–6911. [[CrossRef](#)]
22. Gong, C.; Hu, Y.; Gao, J.; Wang, Y.; Yan, L. An improved delay-suppressed sliding mode observer for sensorless vector-controlled PMSM. *IEEE Trans. Ind. Electron.* **2020**, *67*, 5913–5923. [[CrossRef](#)]
23. Kim, H.; Son, J.; Lee, J. A high-speed sliding-mode observer for the sensorless speed control of a PMSM. *IEEE Trans. Ind. Electron.* **2011**, *58*, 4069–4077.
24. Obeid, H.; Fridman, L.M.; Laghrouche, S.; Harmouche, M. Barrier function-based adaptive sliding mode control. *Automatica* **2018**, *93*, 540–544. [[CrossRef](#)]
25. Zheng, J.; Wang, H.; Man, Z.; Jin, J.; Fu, M. Robust motion control of a linear motor positioner using fast nonsingular terminal sliding mode. *IEEE/ASME Trans. Mechatron.* **2015**, *20*, 1743–1752. [[CrossRef](#)]
26. Ilioudis, V.C. Sensorless control of permanent magnet synchronous machine with magnetic saliency tracking based on voltage signal injection. *Machines* **2020**, *8*, 14. [[CrossRef](#)]
27. Gao, H.; Zhang, G.; Wang, W.; Liu, X. Research on an improved sliding mode sensorless six-phase PMSM control strategy based on ESO. *Electronics* **2021**, *10*, 1292. [[CrossRef](#)]
28. Ye, M.; Shi, T.; Wang, H.; Li, X.; Xia, C. Sensorless-MTPA control of permanent magnet synchronous motor based on an adaptive sliding mode observer. *Energies* **2019**, *12*, 3773. [[CrossRef](#)]
29. Gao, P.; Zhang, G.; Lv, X. Model-free control using improved smoothing extended state observer and super-twisting nonlinear sliding mode control for PMSM drives. *Energies* **2021**, *14*, 992. [[CrossRef](#)]
30. Wu, S.; Zhang, J.; Chai, B. Adaptive super-twisting sliding mode observer based robust backstepping sensorless speed control for IPMSM. *ISA Trans.* **2019**, *92*, 155–165. [[CrossRef](#)]
31. Zhao, Y.; Liu, X.; Yu, H.; Yu, J. Model-free adaptive discrete-time integral terminal sliding mode control for PMSM drive system with disturbance observer. *IET Electr. Power Appl.* **2020**, *14*, 1756–1765. [[CrossRef](#)]
32. Apte, A.; Joshi, V.A.; Mehta, H.; Walambe, R. Disturbance-observer-based sensorless control of PMSM using integral state feedback controller. *IEEE Trans. Power Electron.* **2020**, *35*, 6082–6090. [[CrossRef](#)]
33. Lyu, M.; Wu, G.; Luo, D.; Rong, F.; Huang, S. Robust nonlinear predictive current control techniques for PMSM. *Energies* **2019**, *12*, 443. [[CrossRef](#)]
34. Shao, M.; Deng, Y.; Li, H.; Liu, J.; Fei, Q. Sliding mode observer-based parameter identification and disturbance compensation for optimizing the mode predictive control of PMSM. *Energies* **2019**, *12*, 1857. [[CrossRef](#)]
35. Moreno, J.A.; Osorio, M. Strict lyapunov functions for the super-twisting algorithm. *IEEE Trans. Autom. Control.* **2012**, *57*, 1035–1040. [[CrossRef](#)]